Chemical Science

ROYAL SOCIETY OF CHEMISTRY

EDGE ARTICLE

View Article Online
View Journal | View Issue

Cite this: *Chem. Sci.*, 2023, **14**, 2131

All publication charges for this article have been paid for by the Royal Society of Chemistry

Fluoride-free and seed-free microwave-assisted hydrothermal synthesis of nanosized high-silica Beta zeolites for effective VOCs adsorption†

Zhe Ma,[a] Hua Deng,[bc] Lin Li,[d] Qiang Zhang,[ae] Guangrui Chen,[a] Chang Sun,[a] Hong He *[bcf] and Jihong Yu *[ae]

High-silica Beta zeolites, typically synthesized by hydrothermal synthesis with the assistance of F^- or seeds, are highly important in volatile organic compounds (VOCs) adsorption. Fluoride-free or seed-free synthesis of high-silica Beta zeolites attracts great attention. Herein, highly dispersed Beta zeolites with a size of 25–180 nm and Si/Al ratios of 9–∞ were successfully synthesized by a microwave-assisted hydrothermal strategy. We have for the first time revealed that microwave irradiation can induce the formation of hydroxyl free radicals (•OH), promoting the formation of the Si–O–Si bond. Thanks to the high total surface area, pore volume, and excellent hydrophobicity, the as-prepared pure-silica Beta zeolite presents a higher toluene adsorption capacity in VOCs adsorption compared to other pure-silica Beta zeolites prepared by traditional methods. This work provides a facile avenue for fluoride-free and seed-free synthesis of nanosized high-silica zeolites, promising their important applications in VOCs adsorption.

Received 21st November 2022
Accepted 19th January 2023

DOI: 10.1039/d2sc06389a

rsc.li/chemical-science

Introduction

Beta zeolites (***BEA**) featuring intersecting 12-membered ring channels have occupied an indispensable position in the areas of catalysis, adsorption, and separation.[1–8] Notably, high-silica and pure-silica Beta zeolites exhibit excellent performance in the methanol-to-propene (MTP) reaction,[9,10] gas separation,[11] adsorption of volatile organic compounds (VOCs),[12,13] and microelectronics applications[14,15] due to their weak acidity, high hydrophobicity, high hydrothermal stability, and low dielectric constant.

Beta zeolites are typically synthesized by a hydrothermal method and the as-prepared Beta zeolites possess low Si/Al ratios in the range of less than 100. Recently, several synthetic methods have been developed to break the Si/Al ratio (SAR) limit.[16–19] The fluoride-mediated hydrothermal synthesis method has been developed to synthesize high-silica Beta zeolites taking advantage of the charge balancing effect between F^- ions and organic cations.[20,21] Although high-silica Beta zeolites prepared by this fluoride-assisted approach exhibit high hydrophobicity, the particle sizes of the zeolite products are usually large and mineralizer fluoride is highly toxic.[22,23] Using basic media as a mineralizer, high-silica Beta zeolites (SAR of 100 to infinity) could be also prepared by the seed-assisted hydrothermal method under fluoride-free conditions, in which 5–10 wt% seed addition is necessary.[18,24] Besides, the dry gel conversion (DGC) technique has also been developed to synthesize high-silica Beta zeolites in the absence of fluoride media. However, due to the low migration rate of raw materials, the obtained small crystal particles tend to aggregate during the crystallization process.[25–30] In addition to the TEA^+ cation, certain special organic cations like 4,4-trimethylene-bis(*N*-methyl,*N*-benzyl-piperidinium) could also be employed as an organic structure directing agent (OSDA) cation for synthesizing high-silica Beta zeolites, but the zeolites show low crystallinity.[31,32] The preparation of such special organic cations is complicated and the crystallization time of zeolites is as long as 10 days.[33,34] Wu's group successfully synthesized nanosized high-silica Beta zeolites *via* the interzeolite transformation strategy within a shortened crystallization time, in which the dealuminated **MWW** or **MOR** zeolites were used as the silicon source.[10,35] Nevertheless, this strategy requires the presence of fluoride medium or Beta zeolite seeds. Therefore, developing a simple and efficient seed-free and fluoride-free method to prepare high-silica Beta zeolites is highly desired.

[a]*State Key Laboratory of Inorganic Synthesis and Preparative Chemistry, College of Chemistry, Jilin University, 2699 Qianjin Street, Changchun 130012, P. R. China. E-mail: jihong@jlu.edu.cn*

[b]*Center for Excellence in Regional Atmospheric Environment, Key Laboratory of Urban Pollutant Conversion, Institute of Urban Environment, Chinese Academy of Sciences, Xiamen 361021, China. E-mail: honghe@rcees.ac.cn*

[c]*University of Chinese Academy of Sciences, Beijing 100049, China*

[d]*Electron Microscopy Center, Jilin University, 2699 Qianjin Street, Changchun 130012, P. R. China*

[e]*International Center of Future Science, Jilin University, 2699 Qianjin Street, Changchun 130012, P. R. China*

[f]*Research Center for Eco-Environmental Sciences, Chinese Academy of Sciences, Beijing, 100085, China*

† Electronic supplementary information (ESI) available. See DOI: https://doi.org/10.1039/d2sc06389a

Notably, nanosized high-silica Beta zeolites have been proven to show superior performances over micrometer-sized high-silica Beta zeolites in the MTP reaction[9,10] and the adsorption of VOCs,[18,35] which is due to their shorter diffusion path and larger external surface area.[36] Several preparation methods including two-step hydrothermal synthesis,[37] steam-assisted conversion,[38] seed-induced approach,[39] high-temperature synthesis,[40] and microwave-assisted synthesis[41] have been proven to be effective strategies for nanocrystalline zeolites. Among them, the microwave-assisted synthesis is widely used to prepare nanosized zeolites in a short time, which benefits from the rapid and homogeneous heating of microwave irradiation.[42] Park and co-workers successfully synthesized Beta zeolites within 4 h by microwave-assisted synthesis without fluoride media.[43] In addition, Tang's group reported a microwave-assisted two-step hydrothermal procedure to prepare nanosized Beta zeolites with a uniform particle size of *ca.* 100 nm within 6 h.[44] However, the Si/Al ratios of the nanosized Beta zeolites prepared by microwave-assisted synthesis are usually below 50. To broaden the Si/Al ratios of the nanosized Beta zeolites, our previous work developed a two-step crystallization strategy in the presence of additive L-lysine to prepare nanosized high-silica Beta zeolites (SAR of 6 to 300) with high product yields in a concentrated gel system. But the Beta zeolites with higher Si/Al ratios than 300 cannot be obtained by such a synthetic route.[45] Despite these efforts, the efficient synthesis of high-silica Beta zeolites while maintaining a nano size is still challenging.

Herein, we develop a facile microwave-assisted hydrothermal strategy for preparing nanosized Beta zeolites with a wide Si/Al range from 9 to infinity with the assistance of L-lysine in a concentrated gel system. In this procedure, we demonstrate that microwave irradiation is beneficial not only to reduce the crystal size by the fast heating of the precursor suspension but also to promote the formation of Si–O–Si bonds through inducing hydroxyl free radicals (•OH). In the adsorption of VOCs, the as-prepared pure-silica Beta-∞-180-MW zeolite shows a larger toluene adsorption capacity than the other three pure-silica Beta zeolites prepared by different methods. An effective strategy for seed-free and fluoride-free synthesis of nanosized high-silica Beta zeolites is offered in this work. High total surface area and pore volume, together with excellent hydrophobicity, endow these zeolites with superior adsorption properties.

Results and discussion

Synthesis of nanosized high-silica Beta zeolites

Nanosized high-silica Beta zeolites were synthesized by a microwave-assisted hydrothermal synthesis strategy. The gel compositions were 1.0 SiO_2 : (0–0.05) Al_2O_3 : (0.016–0.047) Na_2O : 0.55 TEAOH : 6 H_2O : 0.2 L-lysine. Typically, the gel mixture was first treated under microwave irradiation at a low temperature (80–100 °C) for 4 h, followed by hydrothermal crystallization at a high temperature (140 °C) for a certain time. Beta-*x*-*y*-MW was used to represent the as-prepared samples, where *x* and *y* indicate their actual Si/Al ratio and particle size, respectively. Table S1† shows the detailed synthetic conditions. As confirmed by powder X-ray diffraction (PXRD) analysis (Fig. 1), these samples present the

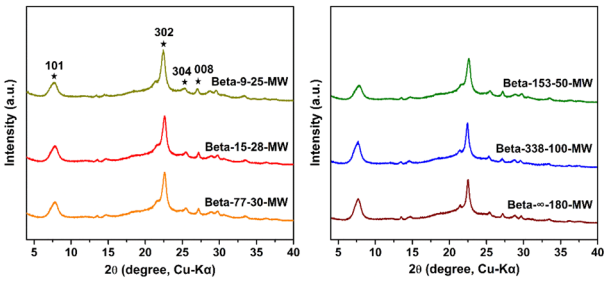

Fig. 1 PXRD patterns of nanosized Beta zeolites with varied Si/Al ratios.

characteristic of ***BEA**-type zeolites, in which the broad diffraction peaks indicate the nanometer size of these Beta zeolite samples.

To explore the crystallization process of the as-prepared samples, a series of Beta zeolites (Beta-15-28- MW, Beta-77-30-MW, Beta-153-50-MW, and Beta-338-100-MW) were synthesized by extending the crystallization time to 48 h during the second hydrothermal step (140 °C). As shown in the PXRD patterns in Fig. S1,† the crystallinities of these four zeolites do not change obviously, indicating that the complete crystallization of Beta zeolites can be achieved in a short time. Based on the above analysis, it can be concluded that well-crystallized Beta zeolites (SAR of 9 to 338) could be rapidly synthesized within 10–14 h using this microwave-assisted hydrothermal synthesis method. Notably, as can be seen from the scanning electron microscopy (SEM) and transmission electron microscopy (TEM) images in Fig. S2 a–e and 2a–e, the as-prepared Beta zeolites exhibit regular morphologies with a uniform nanometer size of *ca.* 25–100 nm, which is consistent with the dynamic light scattering (DLS) results in Fig. S3a–e.† Table S2† summarizes the fast synthesis of Beta zeolites in the literature. The Si/Al ratios of the as-reported Beta zeolites are narrow and their crystal sizes are generally micron-sized. By contrast, the microwave-assisted hydrothermal synthesis strategy in this work shows significant advantages in preparing nanosized Beta zeolites with a wide Si/Al ratio range under seed-free and fluoride-free conditions.

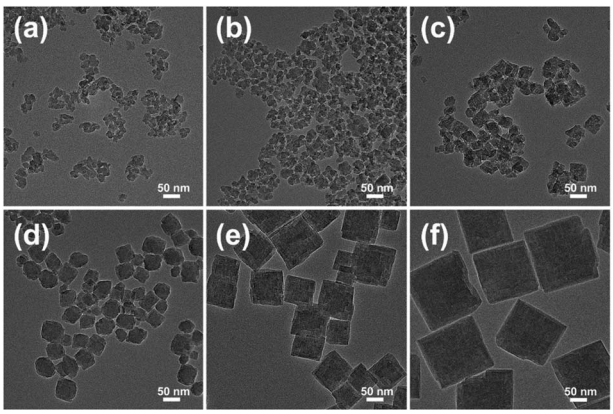

Fig. 2 TEM images of nanosized Beta zeolites with varied Si/Al ratios: (a) Beta-9-25-MW, (b) Beta-15-28-MW, (c) Beta-77-30-MW, (d) Beta-153-50-MW, (e) Beta-338-100-MW, and (f) Beta-∞-180-MW.

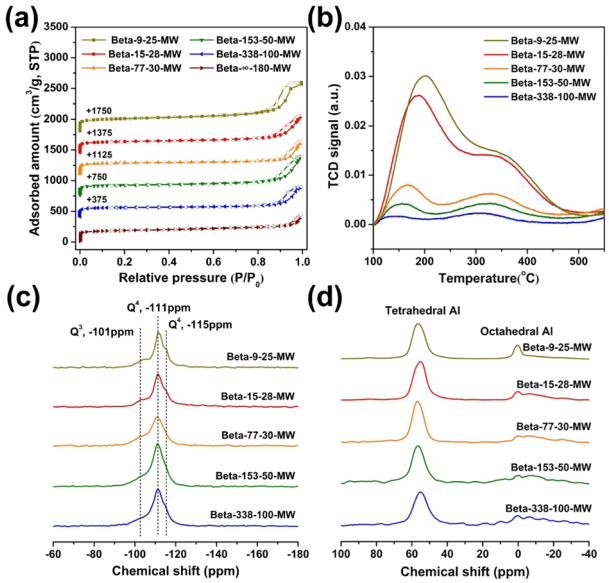

Fig. 3 Structure characterization of nanosized Beta zeolites with varied Si/Al ratios: (a) N_2 adsorption–desorption isotherms, (b) NH_3-TPD profiles, (c) ^{29}Si MAS NMR spectra, and (d) ^{27}Al MAS NMR spectra.

More importantly, we successfully synthesized pure-silica Beta zeolites *via* microwave-assisted hydrothermal synthesis in the absence of seeds and fluoride. Different from the previous microwave-assisted synthesis, in this work, L-lysine was used as a growth modifier and the crystallization was carried out in a concentrated gel system. The SEM and TEM images of pure-silica Beta-∞-180-MW (Fig. S2f† and 2f) present a cubic morphology with a particle size of *ca.* 180 nm (Fig. S3f†). The nanocrystals are highly dispersed, which are smaller than most of pure-silica Beta zeolites reported in the literature (Table S3†).

The structures of Beta zeolites were further characterized and the results are shown in Fig. 3. The N_2 adsorption–desorption isotherms (Fig. 3a) show a steep rise uptake at low P/P_0 pressures, which is typical for microporous materials, and the hysteresis loop at P/P_0 between 0.8 and 1.0 is attributed to the intercrystalline mesopores of nanoparticles. As shown in Table 1, these nanosized high-silica and pure-silica Beta zeolites exhibit a large micropore area and a large micropore volume of 391–422 $m^2\ g^{-1}$ and 0.19–0.20 $cm^3\ g^{-1}$, respectively, indicating their high crystallinities in agreement with the results in PXRD analysis. The acidity of zeolites with varied Si/Al ratios was determined by temperature-programmed desorption of ammonia (NH_3-TPD) (Fig. 3b). With the increase of Si/Al ratios, the total acidities of these zeolites decrease gradually and the high-silica Beta-338-100-MW shows almost no acidity.

^{29}Si MAS NMR results demonstrate that these zeolites contain a large amount of $Q^4((SiO)_4Si)$ units and only a small amount of Q^3 units corresponding to $(SiO)_3Si(OH)$ (Fig. 3c).[35] ^{27}Al MAS NMR results show that most of the aluminum is tetrahedrally coordinated (Fig. 3d).[45] To test the hydrothermal stability of the as-prepared Beta zeolites, the sample Beta-153-50-MW was exposed to 10% water steaming at 750 °C for 3 h. There is no nearly change in the PXRD pattern, N_2 adsorption–desorption isotherms, and TEM image of the sample before and after treatment (Fig. S4–S6†).

Effect of microwave irradiation on the crystallization of nanosized high-silica Beta zeolites

To reveal the effect of microwave irradiation on the preparation of nanosized high-silica Beta, we characterized the crystallization intermediates (Beta-153-50-i and Beta-∞-180-i) after microwave irradiation. As shown by the XRD patterns in Fig. S7†, both Beta-153-50-i and Beta-∞-180-i show amorphous features, indicating that the crystallization has not started yet in the first microwave-irradiation stage, which can be further confirmed by the irregular morphologies of these two samples in the SEM images (Fig. S8†). Notably, many nano-sized metastable nanoparticles (*ca.* 10 nm) are formed during the microwave irradiation stage, as demonstrated by the DLS characterization (Fig. S9†). ^{29}Si MAS NMR spectra show that both intermediates mainly contain $Q^4((SiO)_4Si)$ units (Fig. S10†), indicating that a large amount of Si–O–Si bonds are built in this microwave irradiation stage.

To further investigate the mechanism of microwave-assisted crystallization of nanosized high-silica Beta zeolites, we conducted subsequent electron paramagnetic resonance (EPR) experiments on the initial reaction mixture with or without microwave irradiation and the results are shown in Fig. 4. Typically, the initial

Table 1 Si/Al ratios, particle sizes, and porosities of the as-prepared nanosized Beta zeolites

Sample	Si/Al (initial)	Si/Al[a] (ICP)	Particle size[b] (nm)	S_{BET}[c] ($m^2\ g^{-1}$)	S_{micro}[d] ($m^2\ g^{-1}$)	S_{ext}[d] ($m^2\ g^{-1}$)	V_{micro}[d] ($cm^3\ g^{-1}$)
Beta-9-25-MW	10	9	25	714	422	292	0.20
Beta-15-28-MW	20	15	28	628	412	216	0.20
Beta-77-30-MW	80	77	30	626	418	208	0.19
Beta-153-50-MW	160	153	50	610	406	204	0.19
Beta-338-100-MW	400	338	100	592	391	201	0.19
Beta-∞-180-MW	∞	∞	180	534	410	124	0.19
Beta-14-60-HT	20	14	60	483	339	144	0.16
Beta-72-70-HT	80	72	70	465	361	104	0.20
Beta-123-140-HT	160	123	140	452	335	117	0.18
Beta-265-190-HT	400	265	190	450	284	166	0.17

[a] Measured by inductively coupled plasma-atomic emission spectrometry ICP-AES. [b] Determined based on dynamic light scattering (DLS). [c] S_{BET}: total surface area, calculated by the BET method. [d] S_{micro}: micropore surface area, S_{ext}: mesopore surface area, and V_{micro}: micropore volume, calculated by the *t*-plot method.

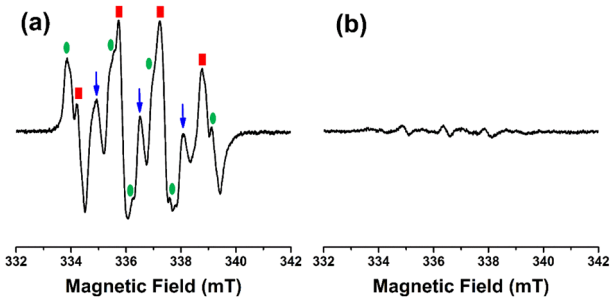

Fig. 4 EPR spectra of the initial reaction mixture containing DMPO: (a) under microwave irradiation and (b) without microwave irradiation. The EPR signals are marked as follows: •OH (red ■); oxidized DMPO radicals (blue ↓); carbon-centered radicals (green •).

synthesis gel was first treated under microwave irradiation at 100 °C for 20 min under 400 W, and then 100 μL of the as-obtained reaction mixture was added into 100 μL of 5,5-dimethylpyrroline-*N*-oxide (DMPO, acted as the spin-trapping agent). Finally, the solution was transferred into an aqueous cell and the EPR data were collected. Strikingly, an obvious quartet pattern is observed in the reaction mixture and the EPR signals corresponding to the DMPO-•OH are significantly strong (Fig. 4a).[46] However, the above characteristic signals did not appear in the reaction mixture without microwave irradiation (Fig. 4b). The results indicate that the hydroxyl radical (•OH) is successfully introduced into the synthesis system of Beta zeolites by microwave irradiation. It has been reported that •OH could be introduced into the synthesis system of zeolites by means of UV irradiation, gamma-ray irradiation, the Fenton reaction, laser photolysis of H_2O_2, *etc.*[47–49] Here, we propose that microwave irradiation can also induce the production of •OH, which is believed to be of great significance for the study of microwave-assisted synthesis of zeolites. Our previous studies reported that the presence of •OH in the synthetic system of zeolites can significantly accelerate the depolymerization of the silica gel by breaking the Si–O bonds and promote the polymerization of the silica species by remaking the Si–O–Si bonds during the nucleation process.[46,50] Based on this, our group successfully synthesized high-silica zeolite Y with a SAR of 6.35 using a hydroxyl radical-assisted strategy.[51] Here, we demonstrate that the introduction of •OH from microwave irradiation can promote the construction of Si–O–Si bonds, which is conducive to break the limitation of the Si/Al ratios of Beta zeolites, thus affording the high-silica or pure-silica Beta zeolites by this microwave-assisted hydrothermal strategy. Besides, a two-step microwave-assisted crystallization was also used to prepare pure-silica Beta zeolites. Typically, the synthesis solution was first treated at 100 °C for 4 h under microwave irradiation and subsequently treated at 160 °C for 10 h under microwave irradiation. As shown in Fig. S11,† the as-prepared product shows an amorphous feature.

In comparison, Beta zeolites with the initial Si/Al ratio from 20 to 400 were synthesized by a two-step hydrothermal synthesis. The gel compositions were 1.0 SiO_2 : (0.00125–0.025) Al_2O_3 : (0.017–0.047) Na_2O : 0.55 TEAOH : 6 H_2O : 0.2 L-lysine. Typically, the hydrothermal crystallization was first performed at a low temperature of 80 °C for 48 h and subsequently at a high temperature of 140 °C for 48 h. Beta-*m*-*n*-HT was used to represent the as-prepared samples, where *m* and *n* indicate their actual Si/Al ratio and particle size, respectively. All the as-prepared samples (Beta-14-60-HT, Beta-72-70-HT, Beta-123-140-HT, and Beta-265-190-HT) present the characteristic diffraction peaks corresponding to ***BEA**-type zeolites as confirmed by PXRD results (Fig. S12†). However, the pure-silica Beta cannot be obtained through this two-step hydrothermal synthesis, as demonstrated by the amorphous feature of the as-prepared product (Fig. S13†). The SEM and TEM images of these four Beta zeolites are shown in Fig. S14 and S15;† it can be seen that they all exhibit regular morphologies and uniform crystal sizes. Their crystal sizes were measured by DLS (Fig. S16†), and the results indicate that the crystal sizes of the samples synthesized by two-step hydrothermal synthesis are more than twice those of the samples prepared by the microwave-assisted hydrothermal strategy. Fig. S17† shows the N_2 adsorption–desorption isotherms of these samples and their textural properties are shown in Table 1. These samples present lower total surface area and pore volume of 450–483 $m^2\ g^{-1}$ and 0.16–0.20 $cm^3\ g^{-1}$, respectively. It can be concluded that the microwave irradiation of the synthesis gel at a low temperature is more conducive to accelerate nucleation and yield nano-sized metastable nanoparticles than the low-temperature hydrothermal method. This is because irradiation can stimulate the fast heating of the precursor suspension, resulting in significant changes of the kinetics of all reactions involved during the crystallization. In addition, we also conducted EPR experiments on the reaction mixture upon the low-temperature hydrothermal reaction for 12–48 h. As shown in Fig. S18,† there are no obvious EPR signals corresponding to the DMPO-•OH in the reaction mixture.

According to the above analysis, the crystallization process on nanosized high-silica Beta zeolites is proposed in Fig. 5. At the initial crystallization stage, microwave irradiation at a low temperature (80–100 °C) accelerates the nucleation by rapid and homogeneous heating of the precursor suspension and thus produces many nano-sized metastable nanoparticles. Meanwhile, microwave irradiation promotes the depolymerization and polymerization of the gel mixture by the introduction of •OH and thus promotes the formation of Si–O–Si bonds during the nucleation process. Subsequently, the nano-sized metastable nanoparticles are rapidly crystallized under hydrothermal conditions at a high temperature (140 °C), resulting in the preparation of high-silica or pure-silica Beta zeolites with uniform nanometer size. During the crystallization process, L-lysine attached to the surfaces of metastable nanoparticles and functioned as a growth inhibitor *via* steric stabilization, which can be proved by the comparative experiments in Fig. S9.†

Synthesis of large-sized pure-silica Beta zeolites *via* traditional synthesis methods

To compare with pure-silica Beta-∞-180-MW prepared by microwave-assisted hydrothermal synthesis, the other three pure-silica Beta zeolites were also synthesized using fluoride-mediated hydrothermal synthesis, basic-mediated steam-assisted conversion, and dealumination of commercial H-Beta (Si/Al = 12.5); the as-prepared samples are denoted as Beta-∞-HF, Beta-∞-SAC and

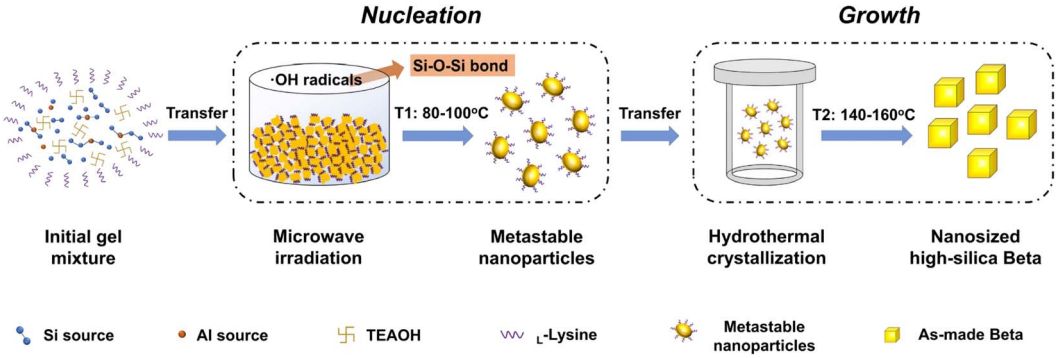

Fig. 5 Crystallization process and the kinetics modulation of Beta zeolite nucleation and growth during the microwave-assisted hydrothermal synthesis.

Beta-∞-DA, respectively. Detailed experimental procedures and synthetic conditions are presented in the ESI.†

The PXRD patterns of these three samples confirmed that they are well-crystallized Beta zeolites and the narrow diffraction peaks indicate their micrometer size (Fig. 6a). It is worth noting that the crystallinity of zeolite Beta-∞-DA is relatively poor. As shown in Fig. S19a and d,† Beta-∞-HF shows a truncated square-bipyramidal morphology and smooth surface with a crystal size of *ca.* 5 μm. In addition, Beta-∞-SAC presents regular cube crystals with a particle size of *ca.* 1 μm (Fig. S19b†). It can be further seen from the high-magnification SEM image that the edge of Beta-∞-SAC is rough, which is caused by the aggregation of small particles during the SAC process (Fig. S19e†). However, Beta-∞-DA zeolite is assembled from 60 to 100 nm crystallites (Fig. S19c and f†). The N_2 adsorption–desorption isotherms of Beta-∞-HF, Beta-∞-SAC, and Beta-∞-DA in Fig. 6b only show a steep rise uptake at low P/P_0 pressures, indicating their microporous structures. The textural properties of these three samples are summarized in Table S4.† Their micropore surface area and micropore volume are 403, 373, 440 $m^2\ g^{-1}$ and 0.17, 0.14, 0.15 $cm^3\ g^{-1}$, respectively, which are lower than those of Beta-∞-180-MW that possesses the smallest crystal size and good crystallinity.

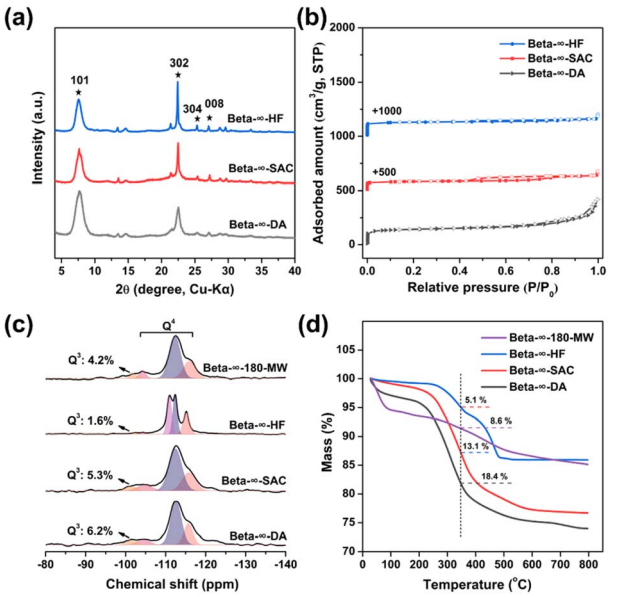

Fig. 6 Structures characterization of pure-silica Beta zeolites synthesized using different methods: (a) PXRD patterns, (b) N_2 adsorption–desorption isotherms, (c) ^{29}Si MAS NMR spectra, and (d) TG curves.

The hydrophilicity/hydrophobicity of Beta-∞-180-MW and the other three pure-silica Beta zeolites were investigated through ^{29}Si MAS NMR spectroscopy and thermogravimetric (TG) analysis. As shown in Fig. 6c, ^{29}Si MAS NMR spectra show a band around −101 ppm associated with $Q^3(SiO)_3Si(OH)$ units and three other bands around −105, −111 (−112), and −115 ppm assigned to Q^4 units corresponding to $((SiO)_4Si)$ sites.[35] As shown in Table S5,† the amount of Q^3 units is in the order of Beta-∞-DA (6.2 wt%) > Beta-∞-SAC (5.3 wt%) > Beta-∞-180-MW (4.2 wt%) > Beta-∞-HF (1.6 wt%), indicating that Beta-∞-HF possesses the fewest defect sites, which is attributed to the electrostatic effects between F^- and TEA^+ and the almost neutral synthesis pH.[20] The TG curves of these four samples are shown in Fig. 6d, in which the weight loss before 350 °C is attributed to the adsorption of water and the weight loss amounts of Beta-∞-180-MW, Beta-∞-HF, Beta-∞-SAC, and Beta-∞-DA are 8.6, 5.1, 13.1, and 18.4 wt%, respectively. With the temperature increase from 350 to 800 °C, Beta-∞-DA shows a maximum weight loss, which is due to the hydroxyl condensation induced by the external surface defect sites. Through measurements of TG and ^{29}Si MAS NMR, it can be concluded that the hydrophobicity of these pure-silica Beta zeolites is in the sequence of Beta-∞-HF > Beta-∞-180-MW > Beta-∞-SAC > Beta-∞-DA.

Adsorption of VOCs over nanosized pure-silica Beta zeolites

Volatile organic compounds such as acetone, *n*-hexane, benzene, toluene, and xylene have caused serious environmental problems and their removal has attracted more and more attention.[52] Among the many effective adsorbents, pure-silica zeolites are an outstanding choice because of their high hydrothermal stability and hydrophobicity.[53] To evaluate the advantages of the nanosized pure-silica Beta-∞-180-MW in adsorption, four pure-silica Beta zeolites were applied in the adsorption of VOCs using toluene as adsorbate. Notably, Fig. 7a and b show the static equilibrium isotherms of water and toluene on the four pure-silica Beta

zeolites. The isotherm curve-fitting parameters are presented in Table S6.† The isotherms of water on the four samples exhibit similar fitting results between Langmuir and Sips models, indicating that the adsorption sites are homogeneous. In contrast, all the isotherm curves of toluene correlate well with the Sips model, indicating that the adsorption of micropores is dominant and the adsorption sites are heterogeneous. As shown in Fig. 7a, the uptakes of water are in the order of Beta-∞-DA (189.62 $cm^3 g^{-1}$) > Beta-∞-SAC (158.08 $cm^3 g^{-1}$) > Beta-∞-180-MW (99.90 $cm^3 g^{-1}$) > Beta-∞-HF (11.02 $cm^3 g^{-1}$). It can be concluded that the hydrophobicity of Beta-∞-180-MW is lower than that of Beta-∞-HF, but higher than those of Beta-∞-DA and Beta-∞-SAC. It can be seen from the isotherms of toluene in Fig. 7b that the adsorption capacities of toluene follow the order of Beta-∞-180-MW > Beta-∞-HF > Beta-∞-SAC > Beta-∞-DA. Notably, Beta-∞-180-MW shows higher toluene adsorption capacity of 124.76 $cm^3 g^{-1}$ than Beta-∞-HF (102.24 $cm^3 g^{-1}$), indicating that the larger pore volume of Beta-∞-180-MW may have an advantage over the stronger hydrophobicity of Beta-∞-HF. In contrast, the adsorption capacity for Beta-∞-SAC (59.22 $cm^3 g^{-1}$) is slightly higher than that for Beta-∞-DA (46.42 $cm^3 g^{-1}$), in which the hydrophobicity is more dominant than pore volume for these two samples.

Furthermore, dynamic adsorption properties were also tested through breakthrough measurement using toluene as adsorbate under humid conditions. It can be seen that the order of dynamic adsorption capacity for these four pure-silica Beta zeolites is Beta-∞-180-MW > Beta-∞-HF > Beta-∞-SAC > Beta-∞-DA (Fig. 7c), which is in agreement with the static equilibrium adsorption results. Afterward, temperature-programmed desorption experiments were performed to confirm dynamic adsorption results. The desorption curves show that the desorption amount of toluene on these four samples is consistent with the adsorption amount (Fig. 7d). Specifically,

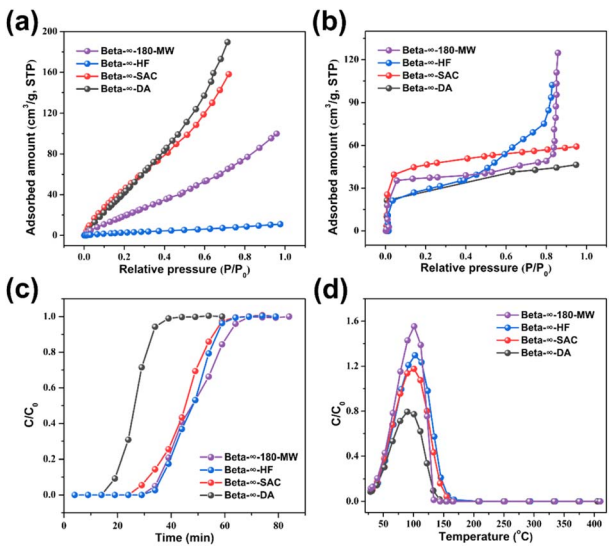

Fig. 7 Adsorption isotherms of water (a) and toluene (b) on four pure-silica Beta zeolites. Breakthrough curves and temperature programmed desorption curves on four pure-silica Beta zeolites: toluene adsorption (c) and desorption (d) under conditions of toluene: 800 ppm, RH = 80%, 30 °C.

Beta-∞-180-MW possessing the largest pore volume and strong hydrophobicity exhibits the highest dynamic adsorption capacity for toluene. The above results indicate that pure-silica Beta-∞-180-MW synthesized by the microwave-assisted hydrothermal strategy is an excellent toluene adsorbent, which is expected to be expanded to adsorption applications of other VOCs.

Conclusions

In summary, a series of nanosized Beta zeolites with a wide Si/Al range from 9 to infinity have been synthesized by a microwave-assisted hydrothermal strategy in the absence of fluoride medium and seed addition. Particularly, Beta zeolites with a Si/Al range of 9–338 can be rapidly synthesized in a short time of 10–14 h while maintaining the nano size of 25–100 nm. Notably, the crystal size of the as-prepared pure-silica zeolite Beta-∞-180-MW is 180 nm, which is much smaller than the pure-silica Beta zeolites prepared by previously reported methods. The two key roles of microwave irradiation in the crystallization process of nanosized high-silica Beta zeolites have been revealed. Microwave irradiation accelerates the nucleation by a rapid heating of the precursor suspension, increasing the number of nucleation sites which has been well documented. Meanwhile, microwave irradiation can induce the production of $^{\bullet}OH$, promoting the formation of Si–O–Si bonds during the nucleation process, which is the first demonstration in this work. Thanks to the high total surface area and pore volume as well as excellent hydrophobicity, the pure-silica Beta-∞-180-MW zeolite shows outstanding VOC adsorption performance outperforming the other three pure-silica Beta zeolites prepared by traditional methods. Such a synthetic strategy is expected to be applied to the synthesis of other nanosized high-silica zeolites and metal-Beta zeolites (*e.g.*, Sn-Beta and Ti-Beta), which may open up a new avenue for the seed-free and fluoride-free synthesis of metal-Beta and high-silica zeolites.

Author contributions

Prof. J. H. Y. conceived the project. Z. M. designed and performed experiments, characterized samples, analyzed data and wrote the manuscript. H. D. performed the VOCs adsorption. L. L. performed TEM images analysis. Q. Z. provided some suggestions to improve the work. G. R. C. and C. S. checked the data. All authors discussed the results and commented on the manuscript. Prof. H. H and J. H. Y. revised the manuscript and finalized the manuscript.

Conflicts of interest

There are no conflicts to declare.

Acknowledgements

We thank the National Natural Science Foundation of China (Grant 22288101, 21835002, and 21920102005), the National Key Research and Development Program of China (Grant

2021YFA1501202, 2022YFA1503600), and the 111 Project (B17020) for supporting this work.

Notes and references

1 M. Treacy and J. Newsam, *Nature*, 1988, **332**, 249–251.
2 J. Higgins, R. B. LaPierre, J. Schlenker, A. Rohrman, J. Wood, G. Kerr and W. Rohrbaugh, *Zeolites*, 1988, **8**, 446–452.
3 Á. Cantín, A. Corma, M. J. Díaz-Cabañas, J. L. Jordá, M. Moliner and F. Rey, *Angew. Chem., Int. Ed.*, 2006, **45**, 8013–8015.
4 C. Chen, J. Zhu, F. Chen, X. Meng, X. Zheng, X. Gao and F.-S. Xiao, *Appl. Catal., B*, 2013, **140**, 199–205.
5 L. Zhang, L. Chen, Y. Li, Y. Peng, F. Chen, L. Wang, C. Zhang, X. Meng, H. He and F.-S. Xiao, *Appl. Catal., B*, 2017, **219**, 200–208.
6 L. Ding, T. Shi, J. Gu, Y. Cui, Z. Zhang, C. Yang, T. Chen, M. Lin, P. Wang and N. Xue, *Chem*, 2020, **6**, 2673–2689.
7 R. Xu, N. Liu, C. Dai, Y. Li, J. Zhang, B. Wu, G. Yu and B. Chen, *Angew. Chem., Int. Ed.*, 2021, **133**, 16770–16776.
8 D. Kaucký, R. Pilař, P. Kukula, J. Bartáček, J. Morávková and P. Sazama, *J. Catal.*, 2022, **407**, 186–197.
9 X. Zhao, L. Wang, P. Guo, N. Yan, T. Sun, S. Lin, X. Guo, P. Tian and Z. Liu, *Catal. Sci. Technol.*, 2018, **8**, 2966–2974.
10 B. Wang, L. Ren, J. Zhang, R. Peng, S. Jin, Y. Guan, H. Xu and P. Wu, *Microporous Mesoporous Mater.*, 2021, **314**, 110894.
11 J. Stelzer, M. Paulus, M. Hunger and J. Weitkamp, *Microporous Mesoporous Mater.*, 1998, **22**, 1–8.
12 L. Zhang, Y. Peng, J. Zhang, L. Chen, X. Meng and F.-S. Xiao, *Chin. J. Catal.*, 2016, **37**, 800–809.
13 M. Jiao, J. Huang, H. Xu, J. Jiang, Y. Guan, Y. Ma and P. Wu, *Angew. Chem., Int. Ed.*, 2020, **59**, 17291–17296.
14 Z. Wang, H. Wang, A. Mitra, L. Huang and Y. Yan, *Adv. Mater.*, 2001, **13**, 746–749.
15 S. Mintova, M. Reinelt, T. Metzger, J. Senker and T. Bein, *Chem. Commun.*, 2003, 326–327.
16 G. Majano, L. Delmotte, V. Valtchev and S. Mintova, *Chem. Mater.*, 2009, **21**, 4184–4191.
17 P. Sazama, E. Tabor, P. Klein, B. Wichterlova, S. Sklenak, L. Mokrzycki, V. Pashkkova, M. Ogura and J. Dedecek, *J. Catal.*, 2016, **333**, 102–114.
18 J. Wang, S. Cao, Y. Sun, X. Meng, J. Wei, Y. Ge, B. Liu, Y. Gong, Z. Li and G. Mo, *ACS Appl. Nano Mater.*, 2021, **4**, 13257–13266.
19 B. Claessens, G. R. Wittevrongel, F. Rey, S. Valencia, J. Cousin-Saint-Remi, G. V. Baron and J. F. Denayer, *Chem. Eng. J.*, 2021, **412**, 128658.
20 M. A. Camblor, A. Corma and S. Valencia, *Chem. Commun.*, 1996, 2365–2366.
21 M. Van den Bergh, A. Krajnc, S. Voorspoels, S. R. Tavares, S. Mullens, I. Beurroies, G. Maurin, G. Mali and D. E. De Vos, *Angew. Chem., Int. Ed.*, 2020, **59**, 14086–14090.
22 X. Zhao, L. Wang, J. Li, S. Xu, W. Zhang, Y. Wei, X. Guo, P. Tian and Z. Liu, *Catal. Sci. Technol.*, 2017, **7**, 5882–5892.
23 Y. Kalvachev, M. Jaber, V. Mavrodinova, L. Dimitrov, D. Nihtianova and V. Valtchev, *Microporous Mesoporous Mater.*, 2013, **177**, 127–134.
24 D. Luo, Q. Wang, D. Fan, M. Yang, B. Fan, K. Cao, S. Xu, P. Tian and Z. Liu, *Microporous Mesoporous Mater.*, 2022, **329**, 111557.
25 P. H. P. Rao, K. Ueyama and M. Matsukata, *Appl. Catal., A*, 1998, **166**, 97–103.
26 P. H. P. Rao, C. L. y Leon, K. Ueyama and M. Matsukata, *Microporous Mesoporous Mater.*, 1998, **21**, 305–313.
27 S. Mintova, V. Valtchev, T. Onfroy, C. Marichal, H. Knözinger and T. Bein, *Microporous Mesoporous Mater.*, 2006, **90**, 237–245.
28 A. Sakthivel, A. Iida, K. Komura and Y. Sugi, *J. Nanosci. Nanotechnol.*, 2009, **9**, 475–483.
29 V. Vattipalli, A. M. Paracha, W. Hu, H. Chen and W. Fan, *Angew. Chem., Int. Ed.*, 2018, **57**, 3607–3611.
30 Y. Luo, M. Li, X. Lv, Q. Huang and X. Chen, *Microporous Mesoporous Mater.*, 2020, **293**, 109675.
31 M. Bregolato, V. Bolis, C. Busco, P. Ugliengo, S. Bordiga, F. Cavani, N. Ballarini, L. Maselli, S. Passeri and I. Rossetti, *J. Catal.*, 2007, **245**, 285–300.
32 O. Larlus, S. Mintova, S. T. Wilson, R. R. Willis, H. Abrevaya and T. Bein, *Microporous Mesoporous Mater.*, 2011, **142**, 17–25.
33 M. Choi, K. Na and R. Ryoo, *Chem. Commun.*, 2009, 2845–2847.
34 R. Martínez-Franco, C. Paris, M. E. Martínez-Armero, C. Martínez, M. Moliner and A. Corma, *Chem. Sci.*, 2016, **7**, 102–108.
35 Z. Zhu, H. Xu, J. Jiang, H. Wu and P. Wu, *ACS Appl. Mater. Interfaces*, 2017, **9**, 27273–27283.
36 M. A. Camblor, A. Corma and S. Valencia, *Microporous Mesoporous Mater.*, 1998, **25**, 59–74.
37 Q. Zhang, G. Chen, Y. Wang, M. Chen, G. Guo, J. Shi, J. Luo and J. Yu, *Chem. Mater.*, 2018, **30**, 2750–2758.
38 T.-L. Cui, J.-Y. He, M. Hu, C.-S. Liu and M. Du, *Microporous Mesoporous Mater.*, 2020, **309**, 110448.
39 B. Xie, H. Zhang, C. Yang, S. Liu, L. Ren, L. Zhang, X. Meng, B. Yilmaz, U. Müller and F.-S. Xiao, *Chem. Commun.*, 2011, **47**, 3945–3947.
40 F. Zhang, L. Zhang, Z. Yang, S. Han, Q. Zhu, L. Wang, C. Liu, X. Meng and F.-S. Xiao, *Chin. J. Catal.*, 2019, **40**, 1093–1099.
41 S.-E. Park, J.-S. Chang, Y. K. Hwang, D. S. Kim, S. H. Jhung and J. S. Hwang, *Catal. Surv. Asia*, 2004, **8**, 91–110.
42 X. Meng and F.-S. Xiao, *Chem. Rev.*, 2014, **114**, 1521–1543.
43 H.-S. You, H. Jin, Y.-H. Mo and S.-E. Park, *Mater. Lett.*, 2013, **108**, 106–109.
44 Y. Hu, C. Liu, Y. Zhang, N. Ren and Y. Tang, *Microporous Mesoporous Mater.*, 2009, **119**, 306–314.
45 Q. Zhang, S. Xiang, Q. Zhang, B. Wang, A. Mayoral, W. Liu, Y. Wang, Y. Liu, J. Shi and G. Yang, *Chem. Mater.*, 2019, **32**, 751–758.
46 G. Feng, P. Cheng, W. Yan, M. Boronat, X. Li, J.-H. Su, J. Wang, Y. Li, A. Corma and R. Xu, *Science*, 2016, **351**, 1188–1191.
47 D. Shi, L. Xu, P. Chen, T. Ma, C. Lin, X. Wang, D. Xu and J. Sun, *Chem. Commun.*, 2019, **55**, 1390–1393.

48 X. Chen, M. Qiu, S. Li, C. Yang, L. Shi, S. Zhou, G. Yu, L. Ge, X. Yu and Z. Liu, *Angew. Chem., Int. Ed.*, 2020, **132**, 11421–11425.
49 J. Wang, Q. Zhang, W. Yan and J. Yu, *Chem. J. Chin. Univ.*, 2021, **42**, 11–20.
50 G. Feng, J. Wang, M. Boronat, Y. Li, J.-H. Su, J. Huang, Y. Ma and J. Yu, *J. Am. Chem. Soc.*, 2018, **140**, 4770–4773.
51 J. Wang, P. Liu, M. Boronat, P. Ferri, Z. Xu, P. Liu, B. Shen, Z. Wang and J. Yu, *Angew. Chem., Int. Ed.*, 2020, **132**, 17378–17381.
52 T. Gelles, A. Krishnamurthy, B. Adebayo, A. Rownaghi and F. Rezaei, *Catal. Today*, 2020, **350**, 3–18.
53 P. Monneyron, M.-H. Manero and J.-N. Foussard, *Environ. Sci. Technol.*, 2003, **37**, 2410–2414.